Sulfur isotopes track the global extent and dynamics of euxinia during Cretaceous Oceanic Anoxic Event 2

Jeremy D. Owens[a,1], Benjamin C. Gill[b], Hugh C. Jenkyns[c], Steven M. Bates[a], Silke Severmann[d], Marcel M. M. Kuypers[e], Richard G. Woodfine[f], and Timothy W. Lyons[a]

[a]Department of Earth Sciences, University of California, Riverside, CA 92521; [b]Department of Geosciences, Virginia Polytechnic Institute and State University, Blacksburg, VA 24061; [c]Department of Earth Sciences, University of Oxford, Oxford OX1 3AN, United Kingdom; [d]Institute of Marine and Coastal Sciences, Rutgers University, New Brunswick, NJ 08901; [e]Max-Planck Institute for Marine Microbiology, 28359 Bremen, Germany; and [f]British Petroleum, Middlesex TW16 7LN, United Kingdom

Edited by Thure E. Cerling, The University of Utah, Salt Lake City, UT, and approved October 8, 2013 (received for review March 21, 2013)

The Mesozoic Era is characterized by numerous oceanic anoxic events (OAEs) that are diagnostically expressed by widespread marine organic-carbon burial and coeval carbon-isotope excursions. Here we present coupled high-resolution carbon- and sulfur-isotope data from four European OAE 2 sections spanning the Cenomanian–Turonian boundary that show roughly parallel positive excursions. Significantly, however, the interval of peak magnitude for carbon isotopes precedes that of sulfur isotopes with an estimated offset of a few hundred thousand years. Based on geochemical box modeling of organic-carbon and pyrite burial, the sulfur-isotope excursion can be generated by transiently increasing the marine burial rate of pyrite precipitated under euxinic (i.e., anoxic and sulfidic) water-column conditions. To replicate the observed isotopic offset, the model requires that enhanced levels of organic-carbon and pyrite burial continued a few hundred thousand years after peak organic-carbon burial, but that their isotope records responded differently due to dramatically different residence times for dissolved inorganic carbon and sulfate in seawater. The significant inference is that euxinia persisted post-OAE, but with its global extent dwindling over this time period. The model further suggests that only ∼5% of the global seafloor area was overlain by euxinic bottom waters during OAE 2. Although this figure is ∼30× greater than the small euxinic fraction present today (∼0.15%), the result challenges previous suggestions that one of the best-documented OAEs was defined by globally pervasive euxinic deep waters. Our results place important controls instead on local conditions and point to the difficulty in sustaining whole-ocean euxinia.

carbonate-associated sulfur | geochemical modeling

The Mesozoic stratigraphic record, particularly the Cretaceous, is populated with numerous intervals of widespread marine organic-rich facies. Because of the approximately coeval stratigraphic occurrence of these organic-rich mudrocks (black shales) in multiple ocean basins, Schlanger and Jenkyns (1) referred to the causative paleoceanographic phenomena as oceanic anoxic events (OAEs). During the OAEs the enhanced burial of organic carbon (OC) led to major perturbations of the carbon cycle (2–4), which is recorded globally as positive isotope excursions in sedimentary organic and inorganic carbon (1, 2). Throughout the Cretaceous, elevated atmospheric carbon dioxide concentrations (5, 6) contributed to high temperatures (7–9). However, during the relatively short time interval of OAE 2 (Cenomanian–Turonian boundary event [∼93.9 Ma]), which lasted ∼500 ka (10–12), there are multiple lines of evidence for fluctuations in atmospheric partial pressure of CO_2 (13, 14), sea-surface temperatures, and redox conditions (13, 15, 16). Such fluctuations are mostly linked to widespread but nonuniform burial of vast amounts of OC (as reviewed in ref. 17) and enhanced continental weathering (18, 19).

Accelerated burial of OC and the accompanying positive carbon-isotope excursion are generally linked to two controls acting singly or in combination: increased primary production (1) and enhanced organic-matter preservation under oxygen-deficient depositional conditions (4). Currently, increased primary production is favored (20) as at least the initial driver, but both mechanisms likely played a role in carbon sequestration that affected the isotopic composition of the ocean–atmosphere system. Furthermore, Cretaceous oceans were primed for major episodes of anoxia and associated carbon burial because of generally elevated temperatures and thus lower oxygen solubility in seawater. A previously unquantified portion of the ocean became sufficiently reducing to allow hydrogen sulfide to accumulate in the water column during OAE 2, leading to at least regionally persistent euxinic conditions (17) marked by organic-rich, laminated black shales across the basins, particularly in the southern portion of the proto-North Atlantic Ocean. Unlike many OAEs in the Mesozoic, OAE 2 has been documented from multiple drill cores and outcrop sections and, in the Indian, Pacific, and Atlantic Ocean basins, at various depths, latitudes, and depositional settings (4). The most renowned lithological manifestation of OAE 2 is the so-called "Bonarelli Level" that crops out in the Marche–Umbrian Apennines of central Italy (1).

Sustained increases in primary production during OAE 2 require at least transient enhanced delivery of nutrients and bioessential metals (N, P, Fe, etc.) to the ocean. Identification of the mechanisms behind such increased nutrient delivery has been a major topic of investigation (21), and three main mechanisms have been proposed: (*i*) hydrothermal activity (22, 23, 24), (*ii*) enhanced continental weathering (18, 19), and (*iii*)

Significance

Oxygen in the atmosphere and ocean rose dramatically about 600 Mya, coinciding with the first proliferation of animals. However, numerous biotic events followed when oxygen concentrations in the younger ocean dipped episodically. The Cretaceous is famous for such episodes, and the most extensive of these oceanic anoxic events occurred 93.9 Mya. Our combined carbon- and sulfur-isotope data indicate that oxygen-free and hydrogen sulfide-rich waters extended across roughly 5% of the global ocean, compared to <<1% today, but with the likelihood that much broader regions were also oxygen challenged. These conditions must have impacted nutrient availability in the ocean and ultimately the spatial and temporal distribution of marine life across a major climatic perturbation.

Author contributions: J.D.O., B.C.G., H.C.J., S.S., M.M.M.K., and T.W.L. designed research; J.D.O., H.C.J., S.M.B., R.G.W., and T.W.L. performed research; J.D.O., B.C.G., R.G.W., and T.W.L. analyzed data; and J.D.O., B.C.G., H.C.J., S.M.B., S.S., M.M.M.K., R.G.W., and T.W.L. wrote the paper.

The authors declare no conflict of interest.

This article is a PNAS Direct Submission.

[1]To whom correspondence should be addressed. E-mail: jowens@whoi.edu.

This article contains supporting information online at www.pnas.org/lookup/suppl/doi:10.1073/pnas.1305304110/-/DCSupplemental.

increased phosphorus recycling due to reduction of iron-bearing phases with bound phosphate (25, 26). The hydrothermal model for supplying Fe is challenged by the assumption of widespread euxinia in the water column and the insolubility of iron under those conditions; not surprisingly, the record of hydrothermal Fe signal does not correlate in a straightforward manner with the distribution of organic-rich facies throughout the entire North Atlantic (20, 27). However, neodymium isotope ratios in fish teeth from the western equatorial Atlantic (Demerara Rise) and the north European Chalk Sea may reflect hydrothermal input from the Caribbean and/or Arctic Large Igneous provinces (23, 28). Alternatively, geochemical box modeling suggests that enhanced P from continental weathering was important for the initiation of OAE 2, followed, as a positive feedback, by its sustained availability due to the widespread reduction of P-bearing iron oxides (29) and more generally enhanced P recycling under anoxic conditions (26).

OAE 2 is the most studied of the oceanic anoxic events, yet considerable gaps remain in our understanding of its causes and effects. Evidence from organic biomarkers from multiple sites in the proto-North Atlantic indicates photic-zone euxinia just before and during OAE 2 (as reviewed in ref. 17), and evidence for local oxygen depletion in seawater has been documented using Mn/Ca (30), I/Ca ratios (31), and trace-metal enrichments (as reviewed in ref. 17). Recent modeling by Monteiro et al. (32) suggests that 50% of the global ocean was anoxic. Nevertheless, the spatial extent of anoxic and more specifically, euxinic deposition, remains poorly constrained, particularly for the Pacific and Indian Oceans. Much of the work to date has focused on the proto-North Atlantic, the Western Interior Seaway (WIS), a handful of Pacific sites, and various continental margins (6). The data are limited, but the equatorial Pacific appears to have been a locus for OC burial (ref. 4 and references therein). Certain, contemporaneous, marginal Pacific sites show evidence for oxic conditions (33, 34), and the redox state of the vast majority of the ocean, specifically the Pacific Ocean, remains unknown. Here, we present sulfate S-isotope data from multiple sites spanning several ocean basins recording OAE 2. By combining our dataset with existing sulfate-S and carbonate-C isotope data, we explore the dynamics of the global sulfur cycle during OAE 2 and ultimately gain a unique global perspective on the extent of euxinic conditions during one of the best-studied OAEs.

Sulfur Biogeochemistry Background

Most studies of the Cretaceous sulfur cycle have focused on broad, 10^8-y secular trends seen in the marine sulfate-S isotope record (35). However, two high-resolution investigations have specifically targeted the sulfur cycle during OAE 2 (36, 37). Much of this past work has focused on regional aspects of sulfur cycling (36, 37), including the possibility of enhanced hydrothermal sulfur delivery to the WIS before OAE 2 (36). We present a comprehensive, geographically widespread sulfate-S isotope data set and apply a numerical box model to constrain the history of the global redox state of the ocean during OAE 2.

The concentration and isotopic composition of the marine sulfate reservoir is a reflection of the inputs and outputs of sulfur to the ocean. The significant inputs are weathering of sulfide- and sulfate-bearing minerals from continental rocks and emissions from volcanic/hydrothermal systems (as reviewed in ref. 38). The magnitudes of these input fluxes vary temporally and spatially, but their isotopic signatures are similar and cluster in a relatively narrow $\delta^{34}S$ (definition below) range of 0–8‰, and it is unlikely that this isotopic range has changed significantly through time. The primary outputs of sulfur from the ocean are through the precipitation and burial of gypsum, organic-S compounds (which may be particularly important during OAEs), and pyrite in sediments. Over geologic time scales, gypsum burial can exert a control on marine sulfate concentrations (39), but this burial mechanism has little effect on the global isotopic composition of seawater sulfate due to the small fractionation (1–2‰) during gypsum precipitation (40). In stark contrast, pyrite burial has a large effect on the isotopic composition of the marine sulfate reservoir (ref. 41 and references therein). The large isotopic offset between pyrite-S and the starting sulfate reflects the preference for lighter sulfur isotopes during microbial sulfate reduction and the concomitant production of isotopically light hydrogen sulfide. This sulfide combines with reactive Fe to form pyrite within the water column or below the sediment/water interface. The isotopic offset between sulfate-S and sulfide ($\Delta^{34}S$) is captured and preserved in the sedimentary pyrite and can be as great as 70‰ (e.g., ref. 42). At times in the geologic past, pyrite burial was the dominant sink for dissolved sulfate (43, 44), especially during episodes of widespread reducing conditions within the ocean, such as OAEs (43, 45). Organic sulfur could be an additional reduced sulfur sink particularly when pyrite formation is limited by the availability of iron (i.e., under euxinic conditions). The isotopic offset between organic S and sulfate is generally less than that of pyrite. Within this framework, shifts to more positive $\delta^{34}S$ values recorded stratigraphically in tracers of ancient seawater, most commonly gypsum (anhydrite), barite, and carbonate-associated sulfate (CAS), reflect enhanced pyrite burial, whereas negative $\delta^{34}S$ shifts indicate the greater relative importance of input fluxes. Ultimately, the size of the seawater sulfate reservoir (and, by association, its residence time) controls the magnitude and the potential rate of isotopic change.

Carbon- and Sulfur-Isotope Trends

The $\delta^{34}S_{CAS}$ profiles from all four sections (Fig. 1) show positive excursions that coincide roughly with the positive carbon-isotope excursion (Figs. 2 and 3). The preevent (baseline) values for all of the sections are between 19‰ and 21‰ (see below). These values are relatively close to the published seawater value of 19.4‰ for the Cenomanian and Turonian based on the analysis of barite collected from open-ocean sediments (35), although the pre-OAE sulfur-isotope values for CAS from the WIS (36) and Italy (37) are less positive (14–16‰). A return to pre-OAE $\delta^{34}S_{CAS}$ values after the event is observed only at Raia del Pedale and South Ferriby, where relatively extended stratigraphic sections are available.

The northernmost section, South Ferriby, shows a relatively stable $\delta^{34}S_{CAS}$ profile (average of 20.7‰) with no obvious positive isotope excursion during the OAE interval (Dataset S1) that corresponds to South Ferriby. A positive shift does, however, occur after the event, with a peak value of 22.1‰. This peak

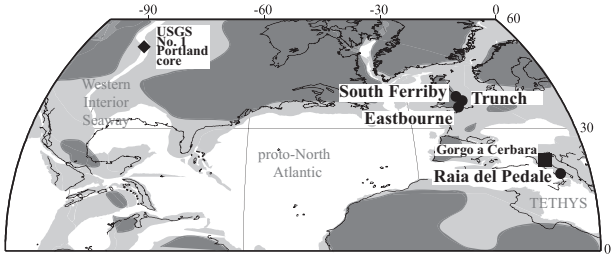

Fig. 1. Paleogeographical reconstruction [generated using GEOMAR (www.odsn.de/odsn/services/paleomap/paleomap.html)] for OAE 2 showing all sample locations used for analysis of CAS sulfur isotopes: (●) locations analyzed in this study, (■) Gorgo a Cerbara (Marche–Umbria, Italy deep-marine Tethyan continental margin) of Ohkouchi et al. (37), and (♦) USGS Portland Core from the Western Interior Seaway of Adams et al. (36). The dark-gray color indicates the landmasses, the light-gray color represents shallow-marine settings, and white designates deep-marine settings for the Late Cretaceous.

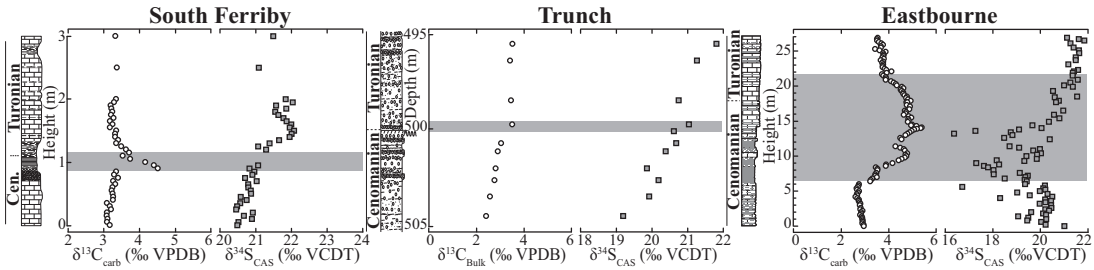

Fig. 2. Chemostratigraphic plots of $\delta^{13}C$ (white circles) and $\delta^{34}S_{CAS}$ (gray squares) for the three UK Chalk sites. The gray bar indicates the previously labeled OAE as defined by the positive carbon-isotope excursion. See *SI Materials and Methods* for further chemostratigraphic details.

coincides stratigraphically with a return to the carbonate carbon-isotope baseline value following the positive excursion. $\delta^{34}S_{CAS}$ values nearly return to the pre-OAE baseline at the top of the section, 1.8 m above the termination level of the OAE.

The next section to the south, Trunch, is the most condensed and has an unconformity just below the OAE interval, although it still captures a significant portion of the upper Cenomanian leading into the OAE. The baseline values at this locality trend more positively before the event, but the average pre-OAE values are typical of those from the other sections (19.4‰). Once again, the most positive $\delta^{34}S_{CAS}$ values (21.8‰) postdate the OAE (as defined by the carbon-isotope data), with a $\delta^{34}S_{CAS}$ excursion of 2.4‰ (Dataset S2) that corresponds to Trunch.

Eastbourne is the southernmost section in the United Kingdom and the most expanded stratigraphically due to comparably high sedimentation rates (46); the OAE spans nearly 10 m of section. This site shows relatively high variability in the $\delta^{34}S_{CAS}$ composition, whereas the $\delta^{13}C_{carb}$ record shows a more systematic increase and subsequent decrease during the OAE. Specifically, the pre-OAE baseline for $\delta^{34}S_{CAS}$ is comparatively stable with an average value of 19.9‰, but there is pronounced variability in the first half of the OAE interval with many of the data points departing from the overall positive trend (*SI Materials and Methods*). The most positive $\delta^{34}S_{CAS}$ value after the event (21.8‰) yields a maximum magnitude for the excursion of 1.9‰, although there is very little available section postdating the OAE (Dataset S3) that corresponds to Eastbourne. Given that the other sites show maxima well after the peak $\delta^{13}C_{carb}$ values, the most positive $\delta^{34}S_{CAS}$ values may not have been captured at this section.

The Italian section, Raia del Pedale, is a shallow-water equivalent to the deep-sea pelagic section that contains the Bonarelli Level black shale characteristic of OAE 2 (17, 37). Importantly, our sample set from Raia del Pedale has the added benefit of high-resolution sampling throughout the entire carbonate section deposited during the OAE, allowing for continuous CAS analysis and stratigraphic coverage that extends well after the event, as determined by the carbonate C- and Sr-isotope records (Fig. 3). The Sr-isotope data from Raia del Pedale can be compared with the long-term composite record (ref. 47 and references therein) to determine the best age correlation for this section following the OAE. Although there is some scatter before the event, the $\delta^{34}S_{CAS}$ baseline at this locality, with an average value of 21.1‰, is similar to preevent data from the other UK sections (Dataset S4) that corresponds to Raia del Pedale. Once again, the peak $\delta^{34}S_{CAS}$ value (25.7‰) occurs stratigraphically well after the $\delta^{13}C_{carb}$ excursion that defines the OAE, and the return to pre-OAE values is captured well after the event. Interestingly, the magnitudes of the positive sulfur-isotope excursions among the various stratigraphic sections suggest a regional trend, with the UK sites showing lower $\delta^{34}S_{CAS}$ values relative to the other sections. Specifically, the average shifts are ~2‰ in the United Kingdom, whereas the section at Raia Del Pedale shows a ~5‰ shift, similar to $\delta^{34}S_{CAS}$ excursion from the WIS and the Italian pelagic deep-sea section that contains the Bonarelli Level (36, 37).

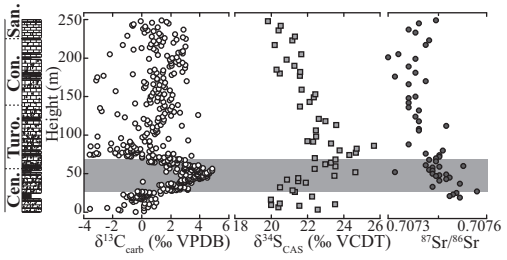

Fig. 3. Chemostratigraphic plot for Raia del Pedale of $\delta^{13}C$ (white circles), $\delta^{34}S_{CAS}$ (gray squares), and $^{87}Sr/^{86}Sr$ (gray circles). The gray bar indicates the previously labeled OAE defined by the $\delta^{13}C$ positive carbon-isotope excursion.

Modeling C and S

The observed carbon- and sulfur-isotope trends demand dramatic perturbations to the geochemical cycles of both elements during OAE 2. To elucidate the coupled dynamics of the carbon and sulfur cycles, we constructed a forward box model. In our model, we prescribed the initial boundary conditions for the two cycles and then perturbed the fluxes until we were able to recreate the observed isotopic excursions, similar to previous studies (36, 41, 43, 45). The initial boundary parameters for the model are given in Table S1. Important but poorly constrained parameters were explored through sensitivity tests (Fig. 4). These influential factors include the magnitude of pyrite fractionation during microbial sulfate reduction ($\Delta^{34}S$), increasing pyrite burial, and initial marine sulfate concentrations. In this model we do not explicitly delineate burial of organic sulfur, which does increase during OAE 2 (48); however, because it represents a reduced sulfur phase, it is lumped with pyrite burial. The difference between pyrite-S and organic-S fractionation relative to the parent sulfate could be a source of some error; however, this assumption does not change our results significantly.

Our model confirms that recreating the observed C- and S-isotope trends can be generated through increasing OC and pyrite burial (Fig. 5). An increase of 1.6× the modern OC flux is necessary to simulate a C-isotope excursion of ~3.5‰ (the approximate average of all published OAE 2 excursions, which range from 2‰ to 6‰, was used for all models). A twofold increase in the total pyrite buried is required to simulate a sulfur-isotope excursion of 5‰. The duration of OAE 2 has been shown to be ~0.5 Ma (10), a time interval that we adopt for all model runs. The magnitude of the excursions can be dampened or amplified by changing the magnitude of OC and pyrite burial, the initial sulfate concentration, and the assumed $\Delta^{34}S$. Note that these modeling results are not unique solutions because of

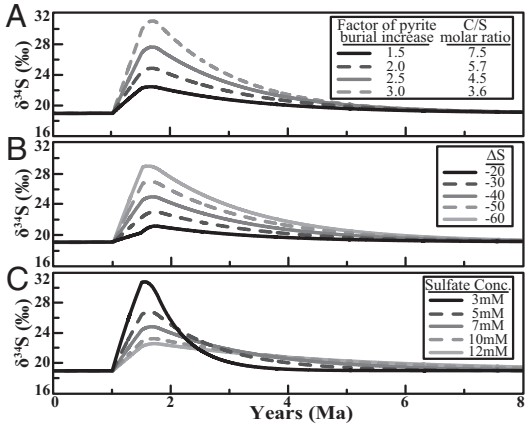

Fig. 4. Sensitivity tests for the modeled sulfur cycle. Here we simulated variations (*A*) in increased pyrite burial and the corresponding C/S ratio, (*B*) increased isotope fractionation during microbial sulfate reduction ($\Delta^{34}S$), and (*C*) initial marine sulfate concentrations. Key parameters were treated the same in each simulation: initial marine sulfate concentration of 7 mM, a twofold increase in pyrite burial, and a change in $\Delta^{34}S$ from −30‰ (non-OAE) to −40‰ during the OAE unless the impact of varying a specific parameter was explored in the simulation.

the high degrees of freedom in key assumptions; they do, however, represent the most plausible circumstances for the generation of the observed geochemical records based on sensitivity tests and observations from the geologic record.

Fig. 4 shows the sensitivity of the model to transient changes in pyrite burial, $\Delta^{34}S$, and initial marine sulfate concentrations. The magnitude of pyrite burial has a large influence on the magnitude of the sulfate isotope excursion captured by $\delta^{34}S_{CAS}$. For example, a 1.5-fold increase in pyrite produces an excursion of ∼3‰, whereas a threefold increase generates a 12‰ excursion (Fig. 4*A*) using an initial sulfate concentration of 7 mM and a $\Delta^{34}S$ of −40‰ during the OAE. We modeled a range of $\Delta^{34}S$ values (−20‰ to −60‰) with a twofold increase in pyrite burial and initial marine sulfate of 7 mM, which predicts a range in the $\delta^{34}S$ excursion of 2–10‰ for seawater sulfate, respectively (Fig. 4*B*). As expected, varying the initial marine sulfate reservoir has an effect on the magnitude of the S-isotope excursion, with 3 mM and 12 mM yielding excursions of 12‰ and 3‰, respectively, based on a twofold increase in pyrite burial and a $\Delta^{34}S$ of −40‰ (Fig. 4*C*).

We also used the model to simulate the observed offset in the C- and S-isotope records. To replicate the observed trends most successfully, we adopt a doubling of pyrite burial during the OAE, a $\Delta^{34}S$ of −40‰, and an initial marine sulfate concentration of 7 mM as our boundary conditions. The value for $\Delta^{34}S$ was chosen based on the global mean $\Delta^{34}S$ defined by an average pre-OAE marine $\delta^{34}S_{sulfate}$ of ∼+20‰ [from average CAS and the barite values of Paytan et al. (35)] and an adjusted average pyrite $\delta^{34}S$ of −20‰. In fact, the average reported pyrite $\delta^{34}S$ values during OAE 2 is ∼-30‰ (35, 47); however, the majority of those data are derived from euxinic localities (which tend to show relatively large fractionations because of dominantly open system, water column pyrite formation). Pyrite formation in euxinic settings generally has larger fractionations that have the potential to exaggerate the global $\Delta^{34}S$ average (41), and the inclusion of organic sulfur would also reduce the global fractionation. Therefore, we use a value of −20‰ for reduced sulfur or, specifically, a $\Delta^{34}S$ of ∼−40‰, reflecting some balance between oxic and euxinic deposition and the importance of organic-S burial during the OAE. The sulfate concentration was chosen based on our model runs—specifically, the length of time for the isotope record to recover to the pre-OAE baseline (see *Global Implication from the Sulfur Cycle* below), and the amount of pyrite buried was determined by reproducing an ∼5‰ excursion.

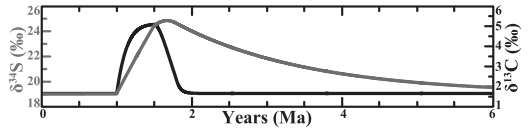

Fig. 5. Modeling of the positive carbon- (black) and sulfur- (gray) isotope excursion, with the gray bar indicating OAE 2 represented from 1.0 to 1.5 Ma as delineated by the characteristic C-isotope profile. In this model the initial marine sulfate concentrations were 7 mM, Δ34S was increased to –40‰, pyrite burial was doubled, and OC burial was increased 1.6-fold during the OAE. The burial of OC and pyrite was decreased progressively, and Δ34S was immediately returned to –30‰ for 300 ka after the OAE.

Global Implication from the Sulfur Cycle

We used a geochemical box model to simulate the observed C- and S-isotope excursions, using sensitivity tests (Fig. 4) to inform the unconstrained variables in the sulfur cycle. This exercise sheds light on the ocean redox evolution during OAE 2. In the modern ocean, euxinic settings cover only ∼0.15% of the seafloor (similar to ref. 49) and bury reduced sulfur at a rate of $\sim 3.1 \times 10^{16}$ mol of sulfur per Ma—mostly in the Black Sea (50). For OAE 2, the entire transient increase in pyrite burial is attributed to increased euxinic deposition, which yields a burial rate of $\sim 4.7 \times 10^{17}$ to 9.3×10^{17} mol of sulfur per Ma during OAE 2 (representing the observed $\delta^{34}S_{CAS}$ excursions of 3–6‰, respectively, with all other parameters held constant as in Fig. 4*A*). These rates equate to 15–30× the modern global flux of euxinic pyrite burial. Assuming conditions during Cretaceous deposition were comparable to those of modern euxinic sites, including mass accumulation rates and Fe availability, our model predicts that roughly 15–30× more of the seafloor was overlain by euxinia during OAE 2. Relative to the 0.15% of euxinic seafloor today, this equates to ∼2.5–5% euxinic deposition during OAE 2. This prediction assumes pyrite burial under oxic and/or oxygen-deficient but noneuxinic environments remained constant throughout the event. In other words, we assume that the entire increase in pyrite burial occurred only within euxinic settings. This assumption is undoubtedly an oversimplification, and any concomitant increase in pyrite burial in oxic and other noneuxinic environments would decrease the estimated extent of euxinia during OAE 2, thus our estimate represents a maximum. Consistent with the possibility of overestimating the extent of euxinia, the negative S-isotope excursions seen in the Eastbourne profile and in the Raia del Pedale profiles close to the onset of the positive carbon-isotope excursion correspond in time with the Plenus Cold Event/Benthic Oxic Event (16), which affected at least the northern hemisphere. This event would have oxidized water-column sulfide where present and marine pyrite, transiently returning isotopically light sulfur to the oceans (*SI Materials and Methods*).

Observations have shown that the southern portion of the North Atlantic was euxinic for much of the event, and the northern portion of the Atlantic appears to show a periodic development of euxinia (as reviewed in ref. 17). Although redox conditions in the Pacific Ocean during the OAE are poorly known, three equatorial sites are documented with increased OC burial (4). Overall, the possibility of transient global expansion of oxygen minimum zones alone could account for the increased areal extent of euxinia during OAE 2 and correlates well with observed OC burial patterns. Whereas our modeled estimate of area of euxinic deposition is much larger than that seen in the modern ocean, the implication is that the majority of the ocean was either oxygen-deficient (but not euxinic) or oxic. Our result, once we also consider the WIS, suggests that euxinia in the Pacific may

have been limited to equatorial regions characterized by high primary productivity and vigorous upwelling and perhaps other regions of coastal upwelling. This reconstruction is much like the modern ocean but likely with overall lower levels of oxygen and far more euxinia spread more broadly across productive regions during OAE 2.

Various factors suggest that our estimate of the increased extent of euxinic deposition might be somewhat conservative. Increases of continental weathering and runoff have been invoked as a mechanism for the enhanced primary production that catalyzed the initiation of OAE 2 (18, 24, 47). Enhanced runoff would also increase the flux of ^{34}S-depleted sulfate to the marine reservoir, and as our model sensitivity test shows (Fig. 4*C*), would thus act to dampen the positive isotope shift caused by increased burial of pyrite. For example, a doubling of continental weathering, while holding all other parameters the same, would require a 2.5-fold increase of pyrite-S to replicate a comparable ∼6‰ δ^{34}S excursion. Using a similar calculation to the one above, such a shift would require ∼7% of the seafloor to have been euxinic, which is not substantially different from our initial estimate of 2.5–5%.

The observed offset between the δ^{13}C and $\delta^{34}S_{CAS}$ positive excursions is a pronounced feature of OAE 2. Previously published sulfate-S data for OAE 2 show a similar pattern (36, 37). On a related note, a more subtle offset is also observed during the Toarcian OAE (45). Only two variables in the model can reproduce this observation: (*i*) an increase in Δ^{34}S fractionation during pyrite burial post-OAE or (*ii*) a slow, simultaneous decrease of OC and pyrite burial. There is evidence, albeit scant, for a Δ^{34}S change during the OAE (36, 48), but there is no evidence for a persistence of higher Δ^{34}S post-OAE; a more likely prediction would be a decrease in Δ^{34}S in the face of lower amounts of euxinic pyrite formation. Therefore, we prescribe a transient increase in Δ^{34}S (−40‰) during the OAE but an immediate return to pre-OAE baseline values following the event (−30‰). More importantly, however, even if Δ^{34}S is held at the OAE value (−40‰) while decreasing OC and pyrite burial (300 ka post-OAE), the model generates a slightly larger offset (∼20 ka). To reproduce the observed offset in the isotope records, the OC and pyrite sulfur burial must be decreased slowly for ∼300 ka after the OAE (from 1.5 to 1.8 Ma in the model) (Fig. 5). The simultaneous waning of OC and pyrite burial has a more immediate effect on the carbon cycle due to its shorter residence time compared with that of sulfur. The starting reservoirs for each element are relatively similar, 3.3×10^{18} mol of inorganic C and 3.16×10^{18} mol (7 mM sulfate) of S, but the input flux for C (25×10^{18} mol/Ma) is an order of magnitude greater than sulfur's (1.50×10^{18} mol/Ma). Using our pre-OAE fluxes and initial marine reservoir concentrations yields C and S residence times of ∼150 ka and ∼2 Ma, respectively. In other words, decreasing extents of euxinia continue to drive the S-isotope excursion heavy, whereas the marine C-isotope compositions rebound faster because the input-to-reservoir ratio is dramatically larger relative to sulfur. The model predicts a small drawdown of sulfate during the OAE, namely a 1-mM decrease based on an initial concentration of 7 mM and doubling of pyrite burial—and so the resulting effect on the residence time of sulfate would be modest (Fig. S1). In sum, the most plausible driver for the observed offset between carbon- and sulfur-isotope ratios are parallel, incremental decreases in OC and pyrite burial after the OAE in the face of very different residence time relationships (see *SI Materials and Methods* for more details).

Additionally, the time it takes the δ^{34}S for sulfate to return to pre-OAE values is strongly tied to the size of the sulfate reservoir. Fig. 4*C* demonstrates that the lower the sulfate concentration the more rapid the return to the pre-OAE baseline. The Raia del Pedale section is the only location with enough stratigraphic coverage to record the full return to the S-isotope baseline after the OAE, which appears to take ∼3–5 Ma. Modeling suggests that a protracted recovery of this duration demands an initial pre-OAE sulfate reservoir of ∼7 mM. This concentration is at the lower limits estimated for marine sulfate for the Late Cretaceous based on fluid inclusions from marine halite (51) but is above the upper limit of 2.1–4mM suggested by Adams et al. (36) for the WIS.

The model predicts a global mean C/S burial ratio of 5.7 (molar ratio) using the 1.6-fold increase in OC burial and two-fold increase in pyrite burial. The modern normal (oxic) marine C/S ratio is ∼7.5, whereas modern euxinic settings exhibit both very low (<2) and high (>10) C/S ratios, where the high C/S ratio is indicative of euxinic settings where pyrite formation is severely limited by the supply of reactive Fe in combination with high organic-matter availability (52). The average modeled C/S ratio of 5.7 is consistent with a global expansion of euxinic pyrite burial with comparatively significant inputs of reactive Fe on a global scale. However, at the local/regional scale, there is appreciable spatial variability in measured C/S ratios, suggesting heterogeneity in reactive Fe inputs (euxinic pyrite formation, by definition, is Fe-limited, and so the amount of pyrite largely reflects the delivery of Fe to the site of deposition). For example, Demerara Rise in the western equatorial Atlantic records an average C/S ratio of ∼12 (48, 53), which suggests that pyrite-S burial was strongly limited by reactive Fe inputs relative to high burial of OC. In contrast, the WIS records an average C/S ratio of ∼2 (54), suggesting, at least locally, somewhat low OC availability and relatively high fluxes of reactive iron, possibly due to increased hydrothermal activity (22, 55). Our calculated mean C/S ratio thus captures the balance between these extremes across the spatial landscape of varying organic production and Fe delivery.

Conclusions

Paired C- and S-isotope records illuminate the timing of environmental change and spatial expansion and contraction of euxinia during OAE 2. Our measurements show that the intersite magnitude of the positive S-isotope excursion during OAE 2 varies from 2‰ to 7‰, whereas the magnitude of the C-isotope excursion varies from 2‰ to 5‰. Modeling of the isotope records suggests that the excursions were driven by increased burial of pyrite and OC. Although generally coupled, these C- and S-isotope excursions show a pronounced offset between peak magnitudes. The observed offset between these isotope signatures may not be unique in the geologic record but is certainly a pronounced characteristic of OAE 2. Our modeling links this relationship to continued euxinic burial of OC and pyrite-S after the OAE proper, but at decreasing rates, with carbon rebounding at a faster rate due to its shorter residence time compared with that of sulfur. The spatial variability in the excursion magnitudes could be due to local watermass differences and/or varying riverine fluxes to an ocean with substantially lower than modern sulfate concentrations, an effect noted also for the Toarcian OAE (56).

The spatial extent of euxinia predicted during OAE 2 is also estimated through our modeling. To reproduce the observed geochemical signatures, the model demands a 15- to 30-fold increase in the area of euxinic deposition during the event: equivalent to ∼2.5–5% of the seafloor. Importantly, this estimate is still relatively small and implies that much of the ocean was devoid of hydrogen sulfide in the water column and was predominantly anoxic (but nonsulfidic), suboxic, and/or oxic. Parallel modeling of trace-metal and isotopic geochemistry could help resolve the global extent of oxygen-deficient settings with sulfide limited to the pore waters and seafloor oxic deposition during the event. Nevertheless, this spatial increase in euxinia during OAE 2 would likely have major implications for other biogeochemical elements, such as Fe and Mo, which could eventually limit primary production and thus trigger the termination of the OAE through feedback processes.

Materials and Methods

We used a CAS extraction method similar to traditional approaches. In summary, 20 g of powdered sample were treated with NaCl and bleach solutions, followed by distilled water rinses. The intent was to remove any sulfate and organic-sulfur compounds that might otherwise be incorporated into the extracted CAS record. The samples were then dissolved with 4 M HCl and filtered to isolate the CAS-bearing solute from the insoluble fraction within 1 h. Through addition of BaCl, the extracted sulfate precipitated as barite, which was then analyzed through on-line combustion using a Thermo Finnigan Delta V Plus continuous-flow stable isotope ratio mass spectrometer at the University of California, Riverside. Further discussion on methods and samples is available in *SI Materials and Methods*.

ACKNOWLEDGMENTS. We thank Bill Gilhooly, Chris Reinhard, and Noah Planavsky for formative discussions. We also thank two anonymous reviewers for thoughtful comments that helped improve and clarify the paper. Samples from the Trunch borehole were obtained courtesy of the British Geological Survey. The US National Science Foundation provided funds for this research (to T.W.L.).

1. Schlanger SO, Jenkyns HC (1976) Cretaceous anoxic events: Causes and consequences. *Geol Mijnb* 55:179–184.
2. Arthur MA, Dean WE, Pratt LM (1988) Geochemical and climatic effects of increased marine organic carbon burial at the Cenomanian/Turonian boundary. *Nature* 335: 714–717.
3. Scholle PA, Arthur MA (1980) Carbon isotope fluctuations in Cretaceous pelagic limestones; Potential stratigraphic and petroleum exploration tool. *AAPG Bull* 64:67–87.
4. Schlanger SO, Arthur MA, Jenkyns HC, Scholle PA (1987) The Cenomanian-Turonian Oceanic Anoxic Event, I. Stratigraphy and distribution of organic carbon-rich beds and the marine δ13C excursion. *Marine Petroleum Source Rocks,* eds Brooks J, Fleet AJ (Geological Society, London), Special Publications, Vol 26, pp 371–399.
5. Berner RA (2006) GEOCARBSULF: A combined model for Phanerozoic atmospheric O2 and CO2. *Geochim Cosmochim Acta: A Special Issue Dedicated to Robert A. Berner* 70: 5653–5664.
6. Takashima R, Nishi H, Huber BT, Leckie M (2006) Greenhouse World and the Mesozoic Ocean. *Oceanography (Wash DC)* 19:82–92.
7. Huber BT, Hodell DA, Hamilton CP (1995) Middle-Late Cretaceous climate of the southern high latitudes: Stable isotopic evidence for minimal equator-to-pole thermal gradients. *Geol Soc Am Bull* 107:1164–1191.
8. Jenkyns HC, Forster A, Schouten S, Sinninghe Damsté JS (2004) High temperatures in the Late Cretaceous Arctic Ocean. *Nature* 432(7019):888–892.
9. Jenkyns HC, Schouten-Huibers L, Schouten S, Sinninghe Damsté JS (2012) Warm Middle Jurassic–Early Cretaceous high-latitude sea-surface temperatures from the Southern Ocean. *Climate of the Past* 8:215–226.
10. Kuhnt W, Luderer F, Nederbragt S, Thurow J, Wagner T (2005) Orbital-scale record of the late Cenomanian-Turonian oceanic anoxic event (OAE-2) in the Tarfaya Basin (Morocco). *Int J Earth Sci* 94:147–159.
11. Voigt S, et al. (2008) The Cenomanian Turonian of the Wunstorf section (North Germany): Global stratigraphic reference section and new orbital time scale for Oceanic Anoxic Event 2. *Newsletters on Stratigraphy* 43:65–89.
12. Sageman BB, Meyers SR, Arthur MA (2006) Orbital time scale and new C-isotope record for Cenomanian-Turonian boundary stratotype. *Geology* 34:125–128.
13. Jarvis I, et al. (2011) Black shale deposition, atmospheric CO2 drawdown, and cooling during the Cenomanian-Turonian Oceanic Anoxic Event. *Paleoceanography* 26: PA3201.
14. van Bentum EC, Reichart G-J, Forster A, Sinninghe Damsté JS (2012) Latitudinal differences in the amplitude of the OAE-2 carbon isotopic. *Biogeosciences* 9:717–731.
15. Forster A, et al. (2008) The Cenomanian/Turonian oceanic anoxic event in the South Atlantic: New insights from a geochemical study of DSDP Site 530A. *Palaeogeogr Palaeoclimatol Palaeoecol* 267:256–283.
16. Gale AS, Christensen WK (1996) Occurrence of the belemnite *Actinocamax plenus* in the Cenomanian of SE France and its significance. *Bull Geol Soc Den* 43:68–77.
17. Jenkyns HC (2010) Geochemistry of oceanic anoxic events. *Geochem Geophys Geosyst* 11:Q03004.
18. Blättler CL, Jenkyns HC, Reynard LM, Henderson GM (2011) Significant increases in global weathering during Oceanic Anoxic Events 1a and 2 indicated by calcium isotopes. *Earth Planet Sci Lett* 309:77–88.
19. Frijia G, Parente M (2008) Strontium isotope stratigraphy in the upper Cenomanian shallow-water carbonates of the southern Apennines: Short-term perturbations of marine $^{87}Sr/^{86}Sr$ during the oceanic anoxic event 2. *Palaeogeogr Palaeoclimatol Palaeoecol* 261:15–29.
20. Jenkyns HC, Matthews A, Tsikos H, Erel Y (2007) Nitrate reduction, sulfate reduction, and sedimentary iron isotope evolution during the Cenomanian-Turonian oceanic anoxic event. *Paleoceanography* 22:PA3208.
21. Meyer KM, Kump LR (2008) Oceanic euxinia in earth history: Causes and consequences. *Annu Rev Earth Planet Sci* 36:251–288.
22. Snow LJ, Duncan RA, Bralower TJ (2005) Trace element abundances in the Rock Canyon Anticline, Pueblo, Colorado, marine sedimentary section and their relationship to Caribbean plateau construction and oxygen anoxic event 2. *Paleoceanography* 20:PA3005.
23. MacLeod KG, Martin EE, Blair SW (2008) Nd isotopic excursion across Cretaceous ocean anoxic event 2 (Cenomanian-Turonian) in the tropical North Atlantic. *Geology* 36:811–814.
24. Pogge von Strandmann PAE, Jenkyns HC, Woodfine RG (2013) Lithium isotope evidence for enhanced weathering during Oceanic Anoxic Event 2. *Nature Geoscience* 6: 668–672.
25. Kraal P, Slomp CP, Forster A, Kuypers MMM (2010) Phosphorus cycling from the margin to abyssal depths in the proto-Atlantic during oceanic anoxic event 2. *Palaeogeogr Palaeoclimatol Palaeoecol* 295:42–54.
26. Van Cappellen P, Ingall ED (1994) Benthic phosphorus regeneration, net primary production, and ocean anoxia: A model of the coupled marine biogeochemical cycles of carbon and phosphorus. *Paleoceanography* 9:677–692.
27. Owens JD, et al. (2012) Iron isotope and trace metal records of iron cycling in the proto-North Atlantic during the Cenomanian-Turonian oceanic anoxic event (OAE-2). *Paleoceanography* 27:PA3223.
28. Zheng X-Y, et al. (2013) Changing ocean circulation and hydrothermal inputs during Ocean Anoxic Event 2 (Cenomanian-Turonian): Evidence from Nd-isotopes in the European shelf sea. *Earth Planet Sci Lett* 375:338–348.
29. Ozaki K, Tajima S, Tajika E (2011) Conditions required for oceanic anoxia/euxinia: Constraints from a one-dimensional ocean biogeochemical cycle model. *Earth Planet Sci Lett* 304:270–279.
30. Pearce MA, Jarvis I, Tocher BA (2009) The Cenomanian-Turonian boundary event, OAE2 and palaeoenvironmental change in epicontinental seas: New insights from the dinocyst and geochemical records. *Palaeogeogr Palaeoclimatol Palaeoecol* 280: 207–234.
31. Lu Z, Jenkyns HC, Rickaby REM (2010) Iodine to calcium ratios in marine carbonate as a paleo-redox proxy during oceanic anoxic events. *Geology* 38:1107–1110.
32. Monteiro FM, Pancost RD, Ridgwell A, Donnadieu Y (2012) Nutrients as the dominant control on the spread of anoxia and euxinia across the Cenomanian-Turonian oceanic anoxic event (OAE2): Model-data comparison. *Paleoceanography* 27:PA4209.
33. Takashima R, et al. (2011) Prevailing oxic environments in the Pacific Ocean during the mid-Cretaceous Oceanic anoxic event 2. *Nat Commun* 2:234.
34. Hasegawa T, et al. (2013) Carbon isotope stratigraphy and depositional oxia through Cenomanian/Turonian boundary sequences (Upper Cretaceous) in New Zealand. *Cretac Res* 40:61–80.
35. Paytan A, Kastner M, Campbell D, Thiemens MH (2004) Seawater sulfur isotope fluctuations in the Cretaceous. *Science* 304(5677):1663–1665.
36. Adams DD, Hurtgen MT, Sageman BB (2010) Volcanic triggering of a biogeochemical cascade during Oceanic Anoxic Event 2. *Nat Geosci* 3:201–204.
37. Ohkouchi N, et al. (1999) Sulfur isotope records around Livello Bonarelli (northern Apennines, Italy) black shale at the Cenomanian-Turonian boundary. *Geology* 27: 535–538.
38. Bottrell SH, Newton RJ (2006) Reconstruction of changes in global sulfur cycling from marine sulfate isotopes. *Earth Sci Rev* 75:59–83.
39. Wortmann UG, Paytan A (2012) Rapid variability of seawater chemistry over the past 130 million years. *Science* 337(6092):334–336.
40. Raab M, Spiro B (1991) Sulfur isotopic variations during seawater evaporation with fractional crystallization. *Chem Geol Isot Geosci Sect* 86:323–333.
41. Kurtz AC, et al. (2003) Early Cenozoic decoupling of the global carbon and sulfur cycles. *Paleoceanography* 18(4):1090.
42. Canfield DE, Farquhar J, Zerkle AL (2010) High isotope fractionations during sulfate reduction in a low-sulfate euxinic ocean analog. *Geology* 38:415–418.
43. Gill BC, et al. (2011) Geochemical evidence for widespread euxinia in the later Cambrian ocean. *Nature* 469(7328):80–83.
44. Hurtgen MT, Arthur MA, Suits NS, Kaufman AJ (2002) The sulfur isotopic composition of Neoproterozoic seawater sulfate: Implications for a snowball Earth? *Earth Planet Sci Lett* 203:413–429.
45. Gill BC, Lyons TW, Jenkyns HC (2011) A global perturbation to the sulfur cycle during the Toarcian Oceanic Anoxic Event. *Earth Planet Sci Lett* 312:484–496.
46. Gale AS, Jenkyns HC, Kennedy WJ, Corfield RM (1993) Chemostratigraphy versus biostratigraphy: Data from around the Cenomanian-Turonian boundary. *J Geol Soc London* 150:29–32.
47. Jones CE, Jenkyns HC (2001) Seawater strontium isotopes, oceanic anoxic events, and seafloor hydrothermal activity in the Jurassic and Cretaceous. *Am J Sci* 301:112–149.
48. Hetzel A, Böttcher ME, Wortmann UG, Brumsack H-J (2009) Paleo-redox conditions during OAE 2 reflected in Demerara Rise sediment geochemistry (ODP Leg 207). *Palaeogeogr Palaeoclimatol Palaeoecol* 273:302–328.
49. Reinhard CT, et al. (2013) Proterozoic ocean redox and biogeochemical stasis. *Proc Natl Acad Sci USA* 110(14):5357–5362.
50. Neretin LN, Volkov II, Böttcher ME, Grinenko VA (2001) A sulfur budget for the Black Sea anoxic zone. *Deep Sea Res Part I Oceanogr Res Pap* 48:2569–2593.
51. Lowenstein TK, Hardie LA, Timofeeff MN, Demicco RV (2003) Secular variation in seawater chemistry and the origin of calcium chloride basinal brines. *Geology* 31: 857–860.
52. Lyons TW, Berner RB (1992) Carbon-sulfur-iron systematics of the upper-most deepwater sediments of the Black Sea. *Chem Geol* 99:1–27.
53. Kraal P, et al. (2009) Pyrite oxidation during sample storage determines phosphorus fractionation in carbonate-poor anoxic sediments. *Geochim Cosmochim Acta* 73:3277–3290.
54. Dean WE, Arthur MA (1989) Iron-sulfur-carbon relationships in organic-carbon-rich sequences; I, Cretaceous Western Interior Seaway. *Am J Sci* 289:708–743.
55. Meyers SR (2007) Production and preservation of organic matter: The significance of iron. *Paleoceanography* 22:PA4211.
56. Newton RJ, et al. (2011) Low marine sulfate concentrations and the isolation of the European epicontinental sea during the Early Jurassic. *Geology* 39:7–10.

Supporting Information

Owens et al. 10.1073/pnas.1305304110

SI Materials and Methods

We present results from four localities in Europe spanning intervals before, during, and after Oceanic Anoxic Event 2 (OAE 2). The sample locations were selected with an eye toward sites that had direct connection to the open ocean and a spatial distribution that encompasses multiple marine basins (Fig. 1). All sample sites have been previously documented to record the OAE 2 interval by means of biostratigraphy, chemostratigraphy (Sr-and C isotopes), or a combination of both (1–5). A comprehensive discussion of the sedimentology, age relationships, and tectonic settings of the sampled localities is already available (2, 5–7). All of the sections are dominated by carbonate lithologies with abundant microfossils, along with some macrofossils, and are characterized by low organic carbon contents (2, 5–7), with one exception. The section at South Ferriby contains a 10-cm-thick organic-rich interval deposited during OAE 2 (2, 4), which was avoided for carbonate-associated sulfate (CAS) analysis. We chose these carbonate sites because they can capture evolving global seawater chemistry, which tracks ocean-scale redox processes. Importantly, because organic-lean sites typically provide lithologic uniformity before, during, and after the OAE, they potentially represent the best isotopic archives of global marine conditions. Briefly, three of the four localities (Eastbourne cliff section, South Ferriby Quarry, and the Trunch borehole: all United Kingdom) illustrate poorly lithified pelagic foraminiferal–nannofossil-rich chalk facies with similar diagenetic histories and consistently good carbonate preservation. The fourth sample site, Raia del Pedale, is a well-lithified platform-carbonate section in southern Italy, rich in rudist fragments and benthic foraminifera and formerly located on the margin of the Tethys Ocean (Fig. 1). Fig. 2 shows lithostratigraphic sections and carbon isotopes for South Ferriby from Jenkyns et al. (4), stratigraphy for Trunch borehole from Jarvis et al. (3) (note $\delta^{13}C$ from bulk pelagic carbonate), and stratigraphic data and carbon isotopes for the Eastbourne section from Tsikos et al. (1).

All samples analyzed for the $\delta^{34}S_{CAS}$ were dominated by high carbonate contents (60–80 wt%). We followed a standard procedure extracting CAS from the carbonate-rich samples (8, 9). Briefly, the samples were trimmed to eliminate weathered surfaces, including surficial Fe oxidation. Then, 10–20 g of powdered sample were treated with NaCl and NaOCl solutions and rinsed with multiple deionized rinses to prevent the incorporation of any non-CAS sulfur-bearing phases. The samples were then dissolved using 4 M HCl and vacuum-filtered less than 1 h later to minimize the pyrite oxidation, which was further limited in the samples by low pyrite and ferric iron concentrations. A $BaCl_2$ solution was added to precipitate sulfate as $BaSO_4$.

The precipitated and homogenized $BaSO_4$ from each sample was loaded into tin capsules with excess V_2O_5 and analyzed for its $^{34}S/^{32}S$ ratio at the University of California, Riverside. Sulfur-isotope ratios were measured using a Thermo Delta V gas-source isotope-ratio mass spectrometer coupled to a Costech 4010 elemental combustion system for on-line sample combustion and analysis. All sulfur-isotope compositions are reported in standard delta notation as per mil (‰) deviation relative to Vienna Canyon Diablo Troilite and were corrected to a suite of international reference materials using a linear regression (e.g., refs. 8, 9) based on replicate analyses of international standards [International Atomic Energy Agency (IAEA) SO-5 [0.49], IAEA SO-6 [−34.05], and NBS 127 [21.1]] agreed to within 0.2‰ of their published values.

C and S Modeling. The values used in the coupled carbon and sulfur model were based on the combination of available geochemical data and on the sensitivity tests (Fig. 4) to help constrain unknown parameters for the sulfur cycle. As previously stated, there are several possibilities to replicate the observed trends by mixing and matching unconstrained parameters, but we have attempted to bracket a few of these factors using data in combination with estimates for these values in the modern cycles. For instance, the $\Delta^{34}S$ used in the model during non-OAE intervals is close to the modern value and was necessary to achieve steady state with the inputs, whereas the ΔS during the OAE itself was chosen based on the known starting sulfate value (~+20‰; ref. 10) and an average pyrite value of −20‰ [the average pyrite value during the OAE based on the available data is ~−30‰ (11–14), but this is exclusively from euxinic settings and we assume a global average closer to −20‰], which provides a $\Delta^{34}S$ of −40‰. Consequently, the $\Delta^{34}S$ is transiently shifted in the model from −30‰ to −40‰ and back to −30‰ for the intervals prior to, during, and after the OAE, respectively. The starting sulfate concentration was based on the length of time it takes for the S-isotope profile of the Raia del Pedale section to indicate recovery to the pre-OAE baseline and seems to fit best with values between 5 and 9 mM and thus we used the average of 7 mM. The values for continental weathering were held constant with the exception of the enhanced weathering scenario (discussed previously), which would only dampen the positive excursion. Therefore, the only parameter to further adjust is the amount of pyrite burial, which can have dramatic effects on the magnitude of the excursion.

To model the carbon isotope excursion in the modeling exercises, all parameters are held constant in the carbon cycle and the burial of organic carbon is increased to 1.6× the pre-excursion rate. For the sulfur cycle portion of the model, we used the values discussed above and increased the pyrite burial rate to 2× the starting rate because it best replicated a 5–6‰ excursion; however, adjusting this value does not affect the offset between the carbon- and sulfur-isotope excursions. Replicating this offset requires a waning of the carbon and sulfur burial rates (shown in Fig. S1). The longer the transient decay back to the pre-OAE baseline burial rates, the larger the offset because of the differences of sizes of dissolved inorganic carbon (DIC) and sulfate reservoirs and relative magnitude of the fluxes in the cycles compared with this reservoir size. Consequently the peak carbon-isotope values occur closer to the time of maximum organic-carbon burial (i.e., near the end of the OAE), but the sulfur excursion continues to rise until the return to normal pyrite burial as seen in Fig. S1.

Eastbourne Sulfur Geochemical Preservation. The $\delta^{34}S_{CAS}$ at this site shows several negative shifts during the first half of the OAE, although the overall trend of the data shows progressively more positive values. Eastbourne shows small negative excursions within the OAE, although the Raia del Pedale section seems to indicate similar features. These negative excursions in the Eastbourne section seem to be correlated with the most positive $\delta^{13}C_{carb}$ values before the slight decreases in carbon-isotope values. It is difficult to pinpoint the exact origin of the negative excursions at Eastbourne but there are three possibilities to explain the observed phenomena: (*i*) later pyrite oxidation skewing the primary CAS signal, (*ii*) enhanced delivery of sulfate, or (*iii*) a paleoceanographic circulation change.

A concern for the validity of the data for CAS has been the oxidation of pyrite either during the burial of the rock, outcrop weathering, or during the chemical extraction of CAS (15, 16). Due to the slight decrease in carbonate concentration leading into the OAE (on average 83 wt% in OAE chalk sediment and ~91 wt% in non-OAE chalk sediment) this could be a concern. With this in mind, we measured the amount of pyrite in most samples postfiltration of the CAS dissolution step and performed a standard chromium chloride extraction (17). The low amounts of pyrite measured for all sections (Fig. S2), with Eastbourne having the highest values but relatively low compared with previously published CAS data sets (8, 9, 18–21), suggest this effect played a limited role during the extraction procedure. In addition, cross-plots of sulfate isotopes and sulfate concentrations against the pyrite concentration show no trends for individual sections (Fig. S2) or all samples combined. Also, CAS isotope vs. pyrite concentration for Eastbourne shows no linear correlation or obvious trends. Linear correlations with pyrite would imply a mixed signal of primary CAS and pyrite-contaminated sulfate (9, 15, 16); therefore, we believe this signal is a primary $\delta^{34}S_{CAS}$ signal.

Geochemical proxies suggest there was an increase of continental weathering during the OAE (22–24) or increased volcanic activity (13), phenomena which could have delivered isotopically depleted sulfur to the marine reservoir. This model seems unlikely, because a simple mass-balance calculation would suggest that a massive delivery of sulfate would have had to enter the system to account for the isotopic shift. Furthermore, there is no evidence for increased marine sulfate concentrations during the OAE that would necessarily have affected all localities equally.

The third possibility for the $\delta^{34}S_{CAS}$ record that the negative excursions observed at Eastbourne are changes in the paleoceanographic circulation patterns due to climatic processes. There is mounting evidence for a cooling episode during the early part of the OAE, not only due to silicate weathering but also to the global burial of organic carbon, thus decreasing atmospheric CO_2 (25–28). The fall in temperature is documented by the paleotemperature proxy tetraether index $(TEX)_{86}$ (29, 30) in the Northern proto-Atlantic and by invasion of boreal faunas (the so-called "Plenus Cold Event") in the north European Chalk Sea (31), both accompanied by excursions in Nd-isotope ratios, suggesting introduction of watermasses of possible Arctic derivation (32–34). In the proto-Atlantic region and the Western Interior Seaway, the invasion of cooler, more oxygenated waters during the same time interval was characterized by population of the seafloor by benthic foraminifera: the so-called "Benthic Oxic Event" (35, 36). Such oxygenated waters as these would have oxidized subseafloor surficial pyrite and introduced isotopically depleted sulfate into the water column and thus lowered the S-isotope composition of ambient seawater.

1. Tsikos H, et al. (2004) Carbon-isotope stratigraphy recorded by the Cenomanian–Turonian Oceanic Anoxic Event: Correlation and implications based on three key localities. *J Geol Soc London* 161:711–719.
2. Schlanger SO, Arthur MA, Jenkyns HC, Scholle PA (1987) The Cenomanian-Turonian Oceanic Anoxic Event, I. Stratigraphy and distribution of organic carbon-rich beds and the marine δ13C excursion. *Marine Petroleum Source Rocks,* eds Brooks J, Fleet AJ (Geological Society, London), Special Publications, Vol 26, pp 371–399.
3. Jarvis I, Gale AS, Jenkyns HC, Pearce MA (2006) Secular variation in Late Cretaceous carbon isotopes: A new Campanian (99.6-70.6 Ma). *Geol Mag* 143:561–608.
4. Jenkyns HC, Matthews A, Tsikos H, Erel Y (2007) Nitrate reduction, sulfate reduction, and sedimentary iron isotope evolution during the Cenomanian-Turonian oceanic anoxic event. *Paleoceanography* 22:PA3208.
5. Parente M, et al. (2008) Stepwise extinction of larger foraminifers at the Cenomanian-Turonian boundary: A shallow-water perspective on nutrient fluctuations during Oceanic Anoxic Event 2 (Bonarelli Event). *Geology* 36:715–718.
6. Wood CJ, Morter AA, Gallois RW (1994) Upper Cretaceous stratigraphy of the Trunch borehole. *Geology of the Country around Great Yarmouth Memoir for 1:50,000 Sheet 162 (England and Wales) with an Appendix on the Trunch Borehole by Wood and Morter*, eds Arthurton RS, Booth SJ, Morigi AN, Abbott MAW, Wood CJ (HMSO, London), pp 105–110.
7. Gale AS, Jenkyns HC, Kennedy WJ, Corfield RM (1993) Chemostratigraphy versus biostratigraphy: Data from around the Cenomanian-Turonian boundary. *J Geol Soc London* 150:29–32.
8. Gill BC, Lyons TW, Jenkyns HC (2011) A global perturbation to the sulfur cycle during the Toarcian Oceanic Anoxic Event. *Earth Planet Sci Lett* 312:484–496.
9. Gill BC, et al. (2011) Geochemical evidence for widespread euxinia in the later Cambrian ocean. *Nature* 469(7328):80–83.
10. Paytan A, Kastner M, Campbell D, Thiemens MH (2004) Seawater sulfur isotope fluctuations in the Cretaceous. *Science* 304(5677):1663–1665.
11. van Bentum EC, et al. (2009) Reconstruction of water column anoxia in the equatorial Atlantic during the Cenomania-Turonian oceanic anoxic event using biomarker and trace metal proxies. *Palaeogeogr Palaeoclimatol Palaeoecol* 280:489–498.
12. Gautier DL (1987) Isotopic composition of pyrite: Relationship to organic matter type and iron availability in some North American Cretaceous shales. *Chem Geol Isot Geosci Sect* 65:293–303.
13. Adams DD, Hurtgen MT, Sageman BB (2010) Volcanic triggering of a biogeochemical cascade during Oceanic Anoxic Event 2. *Nat Geosci* 3:201–204.
14. Böttcher ME, Hetzel A, Brumsack HJ, Schipper A (2006) Sulfur–iron–carbon geochemistry in sediments of the Demerara Rise. *Proceedings of the Ocean Drilling Program. Scientific Results*, eds Mosher, DC, Erbacher, J, Malone, MJ (Ocean Drilling Program, College Station, TX), Vol 207, pp 1–23.
15. Marenco PJ, Corsetti FA, Kaufman AJ, Bottjer DJ (2008) Environmental and diagenetic variations in carbonate associated sulfate: An investigation of CAS in the Lower Triassic of the western USA. *Geochim Cosmochim Acta* 72:1570–1582.
16. Mazumdar A, Goldberg T, Strauss H (2008) Abiotic oxidation of pyrite by Fe(III) in acidic media and its implications for sulfur isotope measurements of lattice-bound sulfate in sediments. *Chem Geol* 253:30–37.
17. Canfield DE, et al. (1986) The use of chromium reduction in the analysis of reduced inorganic sulfur in sediments and shales. *Chem Geol* 54:149–155.
18. Fike DA, Grotzinger JP, Pratt LM, Summons RE (2006) Oxidation of the Ediacaran ocean. *Nature* 444:744–747.
19. Fike DA, Grotzinger JP (2008) A paired sulfate-pyrite $\delta^{34}S$ approach to understanding the evolution of the Ediacaran-Cambrian sulfur cycle. *Geochim Cosmochim Acta* 72: 2636–2648.
20. Wotte T, Strauss H, Fugmann A, Garbe-Schönberg D (2012) Paired $\delta^{34}S$ data from carbonate-associated sulfate and chromium-reducible sulfur across the traditional Lower–Middle Cambrian boundary of W-Gondwana. *Geochim Cosmochim Acta* 85: 228–253.
21. Loyd SJ, et al. (2012) Sustained low marine sulfate concentrations from the Neoproterozoic to the Cambrian: Insights from carbonates of northwestern Mexico and eastern California. *Earth Planet Sci Lett* 339-40:79–94.
22. Blättler CL, Jenkyns HC, Reynard LM, Henderson GM (2011) Significant increases in global weathering during Oceanic Anoxic Events 1a and 2 indicated by calcium isotopes. *Earth Planet Sci Lett* 309:77–88.
23. Frijia G, Parente M (2008) Strontium isotope stratigraphy in the upper Cenomanian shallow-water carbonates of the southern Apennines: Short-term perturbations of marine $^{87}Sr/^{86}Sr$ during the oceanic anoxic event 2. *Palaeogeogr Palaeoclimatol Palaeoecol* 261:15–29.
24. Pogge von Strandmann PAE, Jenkyns HC, Woodfine RG (2013) Lithium isotope evidence for enhanced weathering during Oceanic Anoxic Event 2. *Nat Geosci* 6:668–672.
25. van Bentum EC, Reichart G-J, Forster A, Sinninghe Damsté JS (2012) Latitudinal differences in the amplitude of the OAE-2 carbon isotopic. *Biogeosciences* 9:717–731.
26. Jarvis I, et al. (2011) Black shale deposition, atmospheric CO2 drawdown, and cooling during the Cenomanian-Turonian Oceanic Anoxic Event. *Paleoceanography* 26: PA3201.
27. Barclay RS, McElwain JC, Sageman BB (2010) Carbon sequestration activated by a volcanic CO_2 pulse during Ocean Anoxic Event 2. *Nat Geosci* 3:205–208.
28. Arthur MA, Dean WE, Pratt LM (1988) Geochemical and climatic effects of increased marine organic carbon burial at the Cenomanian/Turonian boundary. *Nature* 335:714–717.
29. Forster A, et al. (2007) Tropical warming and intermittent cooling during the Cenomanian/Turonian oceanic anoxic event 2: Sea surface temperature records from the equatorial Atlantic. *Paleoceanography* 22:PA1219.
30. Sinninghe Damsté JS, et al. (2010) A CO_2 decrease-driven cooling and increased latitudinal temperature gradient during the mid-Cretaceous Oceanic Anoxic Event 2. *Earth Planet Sci Lett* 293:97–103.
31. Gale AS, Christensen WK (1996) Occurrence of the belemnite *Actinocamax plenus* in the Cenomanian of SE France and its significance. *Bull Geol Soc Den* 43:68–77.
32. Zheng X-Y, et al. (2013) Changing ocean circulation and hydrothermal inputs during Ocean Anoxic Event 2 (Cenomanian-Turonian): Evidence from Nd-isotopes in the European shelf sea. *Earth Planet Sci Lett* 375:338–348.
33. Martin EE, MacLeod KG, Jiménez Berrocoso A, Bourbon E (2012) Water mass circulation on Demerara Rise during the Late Cretaceous based on Nd isotopes. *Earth Planet Sci Lett* 327-328:111–120.
34. MacLeod KG, Martin EE, Blair SW (2008) Nd isotopic excursion across Cretaceous ocean anoxic event 2 (Cenomanian-Turonian) in the tropical North Atlantic. *Geology* 36:811–814.
35. Friedrich O, Erbacher J, Mutterlose J (2006) Paleoenvironmental changes across the Cenomanian/Turonian Boundary Event (Oceanic Anoxic Event 2) as indicated by benthic foraminifera from the Demerara Rise (ODP Leg 207). *Rev Micropaleontol* 49:121–139.
36. Keller G, Berner Z, Adatte T, Stueben D (2004) Cenomanian–Turonian and $\delta^{13}C$, and $\delta^{18}O$, sea level and salinity variations at Pueblo, Colorado. *Palaeogeogr Palaeoclimatol Palaeoecol* 211:19–43.

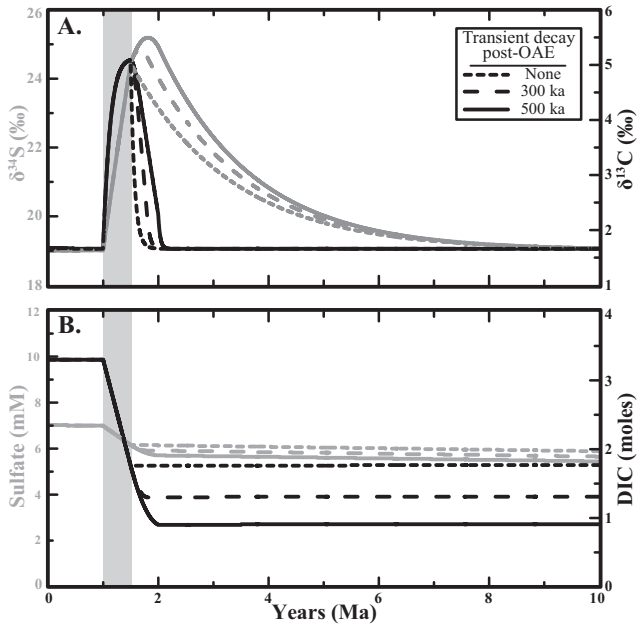

Fig. S1. Sensitivity test for the modeled offset of the coupled carbon and sulfur cycle by varying the amount of time it takes to return to pre-OAE values. This model shows the sensitivity of a waning carbon burial with an increase in the offset of the carbon and sulfur cycles. An increase in time allows for a greater offset and a larger magnitude sulfur-isotope excursion (*A*) whereas having very little effect on the sulfate concentration (*B*). The black lines represent all of the carbon models and blue represents the sulfur models; the dashes for *A* and *B* are shown in the legend of *A*. The models use a twofold increase in pyrite burial, ΔS of −40 during the OAE, and a starting marine concentration of 7 mM.

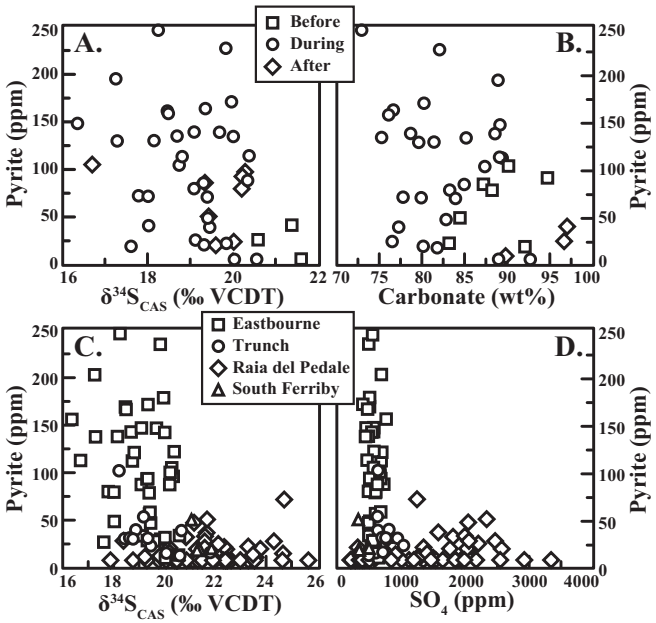

Fig. S2. Cross-plots of geochemical data for Eastbourne (*A* and *B*) and all four sections analyzed in this study (*C* and *D*). In *A* and *B*, pyrite concentrations vs. $\delta^{34}S_{CAS}$ (*A*) and carbonate contents (*B*) show no correlation, indicating that pyrite concentrations have not systematically affected the $\delta^{34}S_{CAS}$ values at Eastbourne. Similarly, *C* and *D* show no correlation for pyrite concentration and $\delta^{34}S_{CAS}$ (*C*) or sulfate concentration (*D*).

Table S1. Initial parameters for the C and S model

Flux (inputs and outputs)	Carbon concentration	$\delta^{13}C$, ‰	Sulfur concentration	$\delta^{34}S$, ‰
Starting marine reservoir	3.3	+1.8	1.35–5.4	+19
Weathering flux	25	−4	0.52* and 0.98†	+5.5
Organic burial	5	−28	—	—
Inorganic burial	20	—	0.67‡ and 0.83§	−11‡ and —§

All fluxes are in 10^{18} mol/Ma, whereas the reservoir sizes are 10^{18} mol. The weathering flux for both cycles combines both the fluxes from volcanic (*) and continental (†) weathering. The isotopic composition of the weathering flux was calculated through isotopic mass balance. The inorganic flux for carbon is based on the burial of carbonates, whereas the sulfur burial portion of the model includes pyrite (‡) and evaporite minerals (§). Em-dashes indicate phases that do not impart a major fractionation on the isotope reservoirs (1), and the $\delta^{34}S$ value for pyrite gives a $\Delta^{34}S$ of −30‰.

1. Kurtz AC, et al. (2003) Early Cenozoic decoupling of the global carbon and sulfur cycles. *Paleoceanography* 18:(4)1090.

Other Supporting Information Files

Dataset S1 (XLS)
Dataset S2 (XLS)
Dataset S3 (XLS)
Dataset S4 (XLS)